minerals

MDPI

Article

Hydrotalcite and Hydrocalumite in Mortar Binders from the Medieval Castle of Portilla (Álava, North Spain): Accurate Mineralogical Control to Achieve More Reliable Chronological Ages

Graciela Ponce-Antón [1,*], Luis Angel Ortega [1], Maria Cruz Zuluaga [1], Ainhoa Alonso-Olazabal [1] and Jose Luis Solaun [2]

[1] Department of Mineralogy and Petrology, Science and Technology Faculty, University of the Basque Country-UPV/EHU, Sarriena s/n, 48940 Leioa, Bizkaia, Spain; luis.ortega@ehu.eus (L.A.O.); mcruz.zuluaga@ehu.eus (M.C.Z.); ainhoa.alonso@ehu.eus (A.A.-O.)

[2] Department of Geography, Prehistory and Archaeology, Faculty of Arts, University of the Basque Country-UPV/EHU, Paseo de la Universidad, 5, 01006 Vitoria-Gasteiz, Spain; joseluis.solaun@ehu.eus

* Correspondence: graciela.ponce@ehu.eus; Tel.: +34-946-015-456

Received: 8 June 2018; Accepted: 26 July 2018; Published: 29 July 2018

Abstract: Mortars from different stratigraphic units at Portilla Castle (Alava, North Spain) have been analyzed for mineralogical characterization before radiocarbon dating. The mortar binder at Portilla Castle is composed not only of neoformation calcite but also of double-layered hydroxide (LDH) minerals such as hydrotalcite and hydrocalumite. The mineralogy of several fractions of the binder has been analyzed to determine the granulometric distribution of minerals in the binder. The continuous monitoring of mineralogy during the extraction of different grain size fractions has been performed by using a scanning electron microscopy (SEM), X-ray diffraction (XRD), and thermogravimetric analyses (TGA). Hydrotalcite and hydrocalumite-bearing mortar binders give older ages than expected since they introduce dead carbon into the system.

Keywords: mortar; binder; hydrotalcite; hydrocalumite; radiocarbon dating

1. Introduction

One of the main goals in building archaeology is to determine the age of the structures discovered. In the absence of written records or other archaeological evidence to establish the chronology of the building, traditionally wooden timbers are used in radiocarbon dating [1]. Through this way, the date obtained may point to older ages due to material reuse or long storage. Therefore, it is vital to determine that the historical remains are not affected by the use of older construction materials since the reuse of wood materials leads to an in-built age defined as the difference between the time when the wood formed and the date of the event of interest [2–5].

In this framework, mortars can provide a potential dating solution. Archaeological mortars are artificial materials composed of a mixture of lime or plaster as binder and sand or other kinds of organic or inorganic additive as aggregates. The ease of preparation as well as the availability of raw materials and their durability have contributed to make mortars ubiquitous materials at sites from the Neolithic period onwards, which becomes an important source of information in archaeological sites [6,7].

Archaeological mortars have been dated by using radiocarbon methods since the 1960s as a way to determine the age of historical/archaeological structures. As such, the application of radiocarbon dating of mortars has been described by several authors [8–21]. Many studies have used charcoal

fragments or other organic inclusions embedded in the mixture to date archaeological mortars. However, the dating of charred materials could provide aged dates by incorporating "dead" C into the system since the calcination process can already be decades or centuries old [22–24].

Lime mortar dating is useful since the mortar binder should reflect the time period when the building was constructed. The basic mortar production technology, known as the lime cycle, can be explained as follows: the calcium carbonate ($CaCO_3$) of the limestone is heated at a high temperature (800–1000 °C) to liberate carbon dioxide (CO_2) and produce quicklime (CaO) in the calcination process (Equation (1)). Then the calcium oxide is slaked by adding water. It then forms portlandite ($Ca(OH)_2$) (Equation (2)). Throughout this phase, portlandite crystals are rearranged and become smaller and foil-like, which enhances their future CO_2 absorption capability [25]. The slaked lime is mixed with aggregates to increase its workability. In the setting phase, the calcium hydroxide in the mortar reacts with atmospheric carbon dioxide and again becomes calcium carbonate in a carbonation process (Equation (3)) [26].

The lime cycle is summarized in the following equations.

$$CaCO_3 \rightarrow CaO + CO_2 \quad (1)$$

$$CaO + H_2O \rightarrow Ca(OH)_2 \quad (2)$$

$$Ca(OH)_2 + CO_2 \rightarrow CaCO_3 + H_2O \quad (3)$$

The ^{14}C of atmospheric carbon dioxide is fixed in the neoformation carbonate as a result of the hardening process and the radiocarbon dating of the binder gives the age of the building. In practice, discrepancies between radiocarbon ages and expected ages are frequently observed. These fluctuations correspond to primary carbonate relicts resulting from the inefficient calcination of the limestone or to carbonate aggregates (limestone fragments) added to the mortar. Those carbonates of different origin are the main problem in radiocarbon dating since they affect the accuracy of results by adding "dead" C to the system and cause an aging of dates [15,18,21,27].

Several methodologies and preparation procedures have been developed to isolate a pure neo-formation calcite fraction without any other carbon contaminant [17–21,28–31]. The first procedures to date the binder consisted of the hydrolysis of lime binder particles of different grain size fractions by using diluted hydrochloric acid (HCl) or 85% ortophosphoric acid (H_3PO_4) [12,13,16,17,19–21,32–35]. When carbonate aggregates appear, mechanical/physical methods of binder extraction are an alternative to chemical methods to avoid contamination by carbonate aggregates in the fraction used for hydrolysis [29,30,36]. The use of lime lumps in mortar for radiocarbon dating has been reported by Van Strydonck et al. [16] and Lindroos et al. [17] since these lumps represent a pure binder when the lime is scarcely mixed with the aggregates [37,38].

However, previously developed protocols do not always solve the problem because often the obtained ages are older or younger than expected. Since the proposed methods do not seem to provide consistent and reproducible results, it is imperative to develop new procedures to assess the contaminant nature and the granulometric distribution within the binder. Since particle size is the main issue to obtain a suitable fraction for dating, the extraction and monitoring of the adequate grain size particle of the binder becomes vital [28].

When dolostones and/or limestones enriched in magnesium are used as a raw material in lime production, magnesium minerals should be considered in the mortar binder because they may add new problems to mortar dating.

During the calcination of calcium magnesium rich limestone, the dolomitic lime cycle differs from the typical lime cycle. When the natural dolomite ($CaMg(CO_3)_2$) is burned, a half thermal decomposition occurs by generating a mixture of periclase (MgO), quicklime (CaO) and calcite ($CaCO_3$) [39]. At the beginning, during the calcination process between 640 °C to 740 °C, the dolomite decomposes to produce calcite ($CaCO_3$) and periclase (MgO) (Equation (4)). Afterward, the generated

calcium carbonate decomposes in quicklime (CaO) (Equation (5)). These reactions are described by the equations below.

$$CaMg(CO_3)_2 \rightarrow CaCO_3 + MgO + CO_2 \quad (4)$$

$$CaCO_3 \rightarrow CaO + CO_2 \quad (5)$$

As a result of the slaking process, besides portlandite ($Ca(OH)_2$), the brucite ($Mg(OH)_2$) mineral phase is also formed, which leads to a wider variety of phases during the carbonation process of the mortar binder.

In comparison with the carbonation of portlandite to calcite, the carbonation of brucite is not simple. Brucite is a relatively stable compound that causes a slow carbonation process and even yields partial carbonation. The resulting mortars contain a mixture of compounds in varying amounts. Therefore, the dolomitic lime cycle does not constitute a full cycle like the calcium lime cycle [40].

Likewise, during the slaking process in the dolomitic cycle, layered double hydroxide (LDH) compounds can be formed [41]. In general, LDH minerals are often referred to as hydrotalcite-like clay (HT-like) since hydrotalcite is one of the most representative minerals in this group [42,43]. The presence of Al^{3+} ions combining with Mg^{2+} ions from MgO leads to the formation of hydrotalcite crystals [$Mg_6Al_2(CO_3)(OH)_{16}{\cdot}4(H_2O)$] [44]. The MgO-$Al_2O_3$ rehydrates and combines with other available anions present in the putty to form hydrotalcite in the presence of water [45,46].

A hydrotalcite mineral is based on positive brucite-like layers alternating with layers containing anions and water molecules. In the crystallographic structure of hydrotalcite, some Mg^{2+} cations are replaced isomorphously by Al^{3+} cations in octahedral sites. The resultant positive charge is balanced by CO_3^{2-} anions in the interlayer sites where the crystallization water can also be found [47–50].

Under hyper-alkaline conditions during the slaking process, Ca^{2+} ions are sparingly soluble [51,52]. Over time, early-formed portlandite is consumed, which forms more stable Ca minerals [53]. In the presence of aluminate ions ($Al(OH)^{4-}$) from the decomposition of clay minerals present as impurities in the raw material, the portlandite ($Ca(OH)_2$) is transformed into some forms of LDH minerals such as hydrocalumite [$Ca_4Al_2(Cl,CO_3,OH)_2(OH)_{12}{\cdot}4H_2O$] [54,55]. Therefore, hydrocalumite is the calcium analogue of hydrotalcite [50,56]. Consequently, these LDH minerals have a high capacity to capture large anions such as CO_3^{2-} due to their ion-exchange properties [47].

LDH phases have been observed in ancient hydraulic mortars, in modern pozzolanic cements, and in dolomitic lime mortars [57–60]. Nevertheless, until the current study, neither the shape nor the size distribution of hydrotalcite and hydrocalumite in the lime mortars has ever been described in detail. To this end, it is essential to establish particle size distribution of mineral phases in the binder. For this purpose, several size grain fractions of the binder have been extracted by a settling procedure and by checking the mineralogy of all fractions using multi-analytical techniques.

The aim of this work is to study mineral composition of the mortar binder obtained by the calcination of dolostones and/or impure limestones in order to select the adequate fraction to date. Several mortar samples from the main structures of Portilla Castle (Álava, Spain) have been analyzed by adapting previous extraction procedures to the real mineralogy.

2. Archaeological Background

The archaeological site of Portilla is located in the village of Zambrana (Álava, Spain) (Figure 1). Portilla Castle and the Portilla de Ibda medieval village form the archaeological site. The site was classified as Cultural Heritage with the category of Monumental Complex in 2012 because it constitutes one the best-conserved examples of a fortified medieval settlement. The archaeological work showed discontinuous periods of occupation during the Late Bronze and Early Iron Ages, the Late Roman Period (3rd to 5th centuries AD), and the Late Middle Ages (11th to 15th centuries).

Portilla Castle is located on Txulato Mountain and the strategic location was valuable for the Kingdom of Navarre during the 11th and 12th centuries until, in the 13th century, it became part of the

Kingdom of Castile. In the early 14th century, the fortified village gradually lost its population as a more accessible settlement was established in the valley. Although the first written references to Portilla date back to the year 1040, the origin and later evolution of the building remains unknown [61,62].

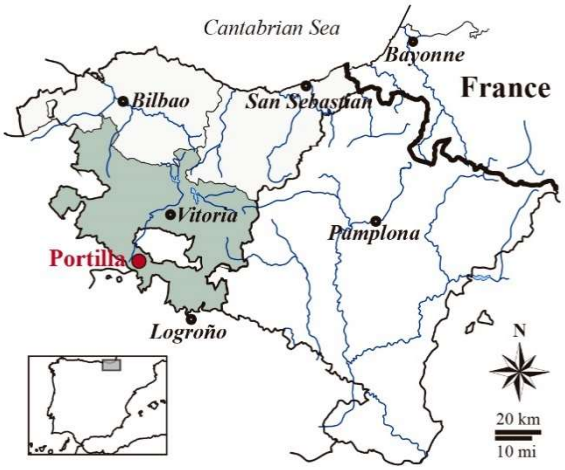

Figure 1. Geographic location of Portilla Castle (Álava, Spain).

3. Materials and Methods

Seven samples of archaeological mortars from different stratigraphic units (SU) at Portilla Castle were considered for lime mortar sampling. Of the fourteen structures defined [62], the three most significant structures were selected in the sampling known as the West Tower (A14, SU-2), Tower Keep (A12, SU-4), and the East Tower (A11, SU-19) (Figure 2 and Table 1).

Figure 2. Studied structures at Portilla Castle. West Tower (A14), Tower Keep (A12), and East Tower (A11).

Table 1. Studied samples from different structures at Portilla Castle.

Stratigraphic Unit	Archaeological Structure	Sample
SU-2	West Town (A14)	CP-2
SU-4	Tower Keep (A12)	CP-4 CP-13-6 CP-13-8 CP-13-10
SU-19	East Town (A11)	CP-19 CP-13-3

SU: Stratigraphic Unit.

To determine the binder and aggregate types, mortar thin-sections were analyzed by an optical polarizing microscope using a Nikon Eclipse LV100POL microscope equipped with a DS F-I1 digital camera and a DS L-2 control unit.

The binder was analyzed by several techniques. The X-ray diffraction (XRD) analysis in a powder sample was performed using a Philips X'Pert diffractometer (Malvern PANalytical, Almelo, The Netherlands) equipped with a monocromatic Cu-$k_{\alpha 1}$ X-radiation operating at 40 kV and 20 mA. The data collection on the powder sample was performed by a continuous scan in the range 5° to 70° [2θ] at an acquisition rate of 0.02° per second [2θ]. The interpretation of diffraction patterns and semi-quantitative calculation were performed with X'Pert HighScore Plus 3.0 software (Malvern PANalytical, Almelo, The Neatherlands) by using a PANalytical on the basis of the characteristic space of each mineral by reconstructing mineral profiles of the compounds and comparing the experimental peaks with experimental patterns of ICDD and ICSD diffraction databases. The extracted fractions of the binder were analyzed by using the scanning electron microscopy (SEM) with a JEOL JSM-7000F Schottky-type field emission scanning electron microscope (JEOL, Tokyo, Japan) and by operating with an Oxford Pentafet photon energy instruments Link Isis X-ray (EDX) microanalysis system. Samples were carbon-coated to eliminate charging effects. Thermo-gravimetric analysis (TGA) was performed in a TA SDT 2960 TG-DSC simultaneous instrument (TA Instruments, New Castle, DE, USA). Pt crucibles containing 5 mg to 7 mg of the sample were heated at 2 °C min^{-1} from room temperature to 1000 °C under a dry oxidizing atmosphere. The samples have been dated by the ^{14}C accelerator technique (AMS) in Beta Analytic Inc. (Miami, FL, USA). The conventional ^{14}C ages were calibrated by using OxCal v4.2.3 software [63] and an IntCal13 atmospheric calibration curve [64].

Extraction Procedure

A settling extraction procedure has been performed to obtain different grain size fractions of the binder based on the procedure described by Ortega et al. [28]. In order to assess the potential of the binder as a time record, the extracted fractions have been characterized mineralogically. Unlike in Ortega et al. [28], the mortars from Portilla Castle show a more complex mineralogy in the finest fraction (<2 μm). The occurrence of potential contaminant phases such as LDHs has led to an adjustment of the extraction procedure to refine the fraction suitable for dating. The modification of the procedure consists of both modifying centrifugation times and including an additional extraction step. The modified extraction procedure of the fractions consists of the following steps (Figure 3).

1. The few upper millimeters of mortar surface were removed using a scraper to eliminate the altered surfaces that may interfere in the analytical results. Then mortars were crumbled manually, which is described by Casadio et al. [65]. The fragments of charcoal produced during lime production were picked out and removed.
2. The sample was placed in an ultrasonic bath with 150 mL of ultrapure water for 10 min. To promote further crumbling, the test tube was shaken vigorously and then left to rest for 5 min.

Then, the topmost 50 mL of suspended volume corresponding to particle fraction size 2 μm to 20 μm was extracted. This fraction was referred to as coarse fraction (CF).

3. Coarse fraction enriched in the binder was re-suspended in 65 mL of ultrapure water and placed in the ultrasonic bath to promote particle disaggregation. The suspension was centrifuged for 100 s at 1000 rpm. The uppermost 15 mL were collected corresponding to a grain size fraction of <2 μm and were referred to as a fine fraction (FF).
4. From the fine fraction, the particles of grain size <0.5 μm were removed. To this end, the sample was re-suspended again in 65 mL of ultrapure water and placed in an ultrasonic bath. The suspension was centrifuged for 9 min at 2000 rpm and the uppermost 15 mL were collected and referred to as ultrafine fraction (UF).
5. The suitable fraction enriched in neoformation calcite was obtained as a result of removing the ultrafine fraction (UF) from the fine fraction (FF). This fraction was named a target fraction (TF) corresponding to a grain size between 0.5 μm to 2 μm.
6. The collected fractions were concentrated via centrifugation at 3000 rpm for 10 min using a Kubota 3000 centrifuge (Kubota Corp., Tokyo, Japan).

To avoid the precipitation of calcite during the extraction process by absorption of modern atmospheric CO_2, ultrapure water was used throughout the process. Moreover, the water is buffered at pH = 8 to preclude the calcite dissolution and favor the optimal scattering of small crystals [66] and, at the same time, avoid chemical reactions that dissolve the calcite [67]. Furthermore, 30 mL of each collected fraction (CF, FF, UF, and TF) were placed in a Petri dish to monitor fraction grain size by several analytical techniques in order to determine the mineralogical composition throughout the procedure. The fractions were dried in an oven at 80 °C. According to the binder/aggregate relation of mortars, the procedure was repeated as necessary until a sufficient amount of the binder for accelerator mass spectrometry (AMS) analysis (>0.8 mg) was obtained.

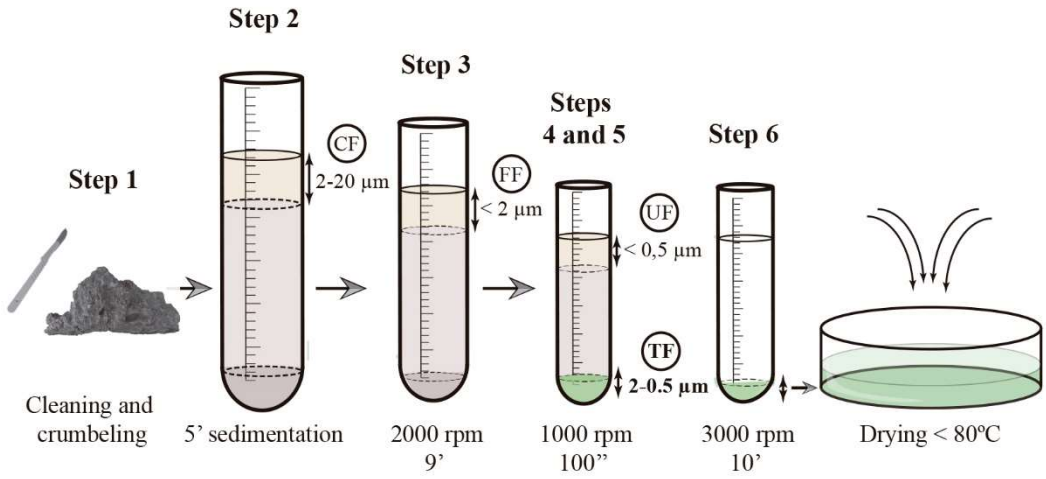

Figure 3. Extraction procedure to obtain the target fraction. Steps 2 to 5 show the mechanical separation of different particle-fractionations of the binder mortar and Step 6 shows the concentration of the extracted fraction. CF: coarse fraction, FF: fine fraction, UF: ultrafine fraction, TF: target fraction.

4. Results and Discussion

Petrographic studies of mortar have been used to identify the nature of aggregates and the binder. The relation and ratios between the aggregates and cementing matrix, texture, form, and size of mortar components have also been observed. The petrographic study of the Portilla samples revealed the similar nature of all the mortars but revealed heterogeneous textures. Aggregates were composed by heterometric and angular/sub-angular detrital quartz, limestone fragments, some

partially dolomitized, and unburnt limestone remains (Figure 4a,b). Within the binder matrix, heterometric lime lumps were observed (Figure 4c,d). Additionally, minute charcoal fragments were present in most samples (Figure 4d). Textural and mineralogical heterogeneities constituted additional difficulties for the extraction of the binder.

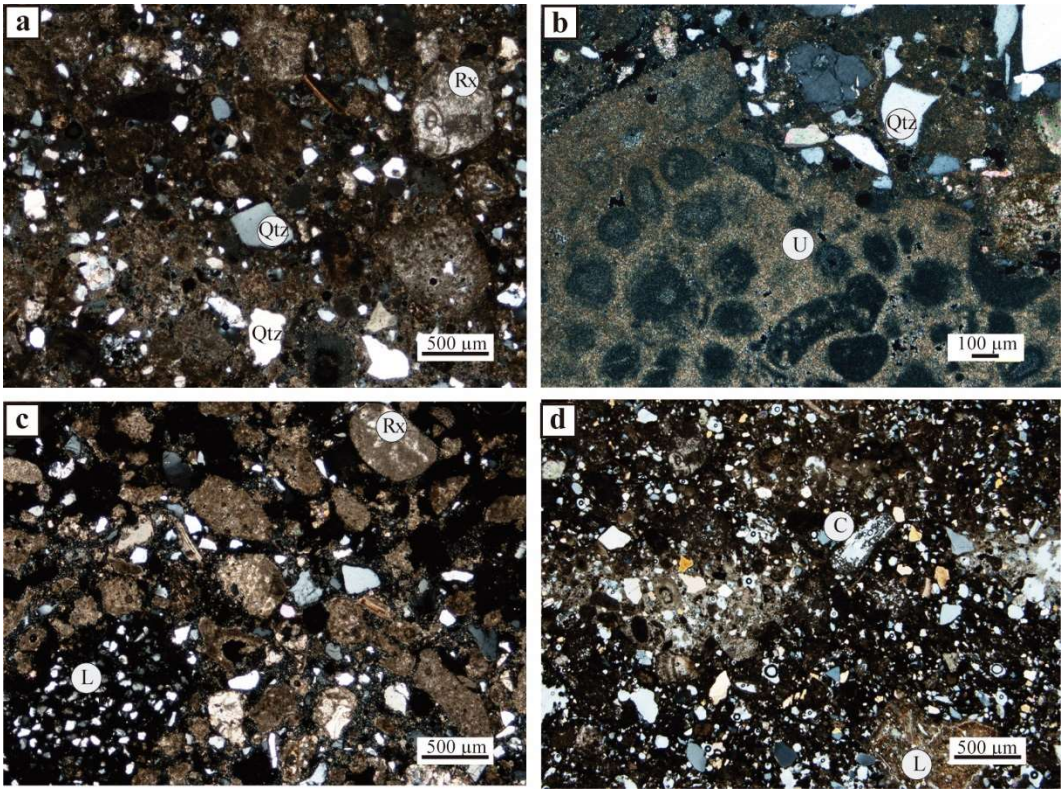

Figure 4. Photomicrographs showing the textural heterogeneity of historic lime mortars from Portilla Castle. (**a**) Mortar with rock fragments, lumps, and quartz grains. (**b**) Fragments of unburnt limestone and angular quartz grains. (**c**) Mortar with limestone fragments and quartz bearing lumps. (**d**) Mortar with a pure lump and charcoal fragment. Rx: rock fragment, Qtz: quartz, L: lump, U: unburnt, C: charcoal.

During the binder extraction process, several analytical techniques were applied to evaluate the mineralogy of the different fractions and monitoring the extraction method. By XRD analysis of the fine fraction (<2 µm), magnesium calcite was identified as the main component of all samples while quartz, hydrotalcite [$Mg_6Al_2(CO_3)(OH)_{16}{\cdot}4(H_2O)$], and hydrocalumite [$Ca_4Al_2(Cl,CO_3,OH)_2(OH)_{12}{\cdot}4H_2O$] are also present in minor amounts (Figure 5). The low intensity of hydrotalcite and hydrocalumite reflections indicates not only low abundance but also the low degree of crystallization of these mineral phases [49].

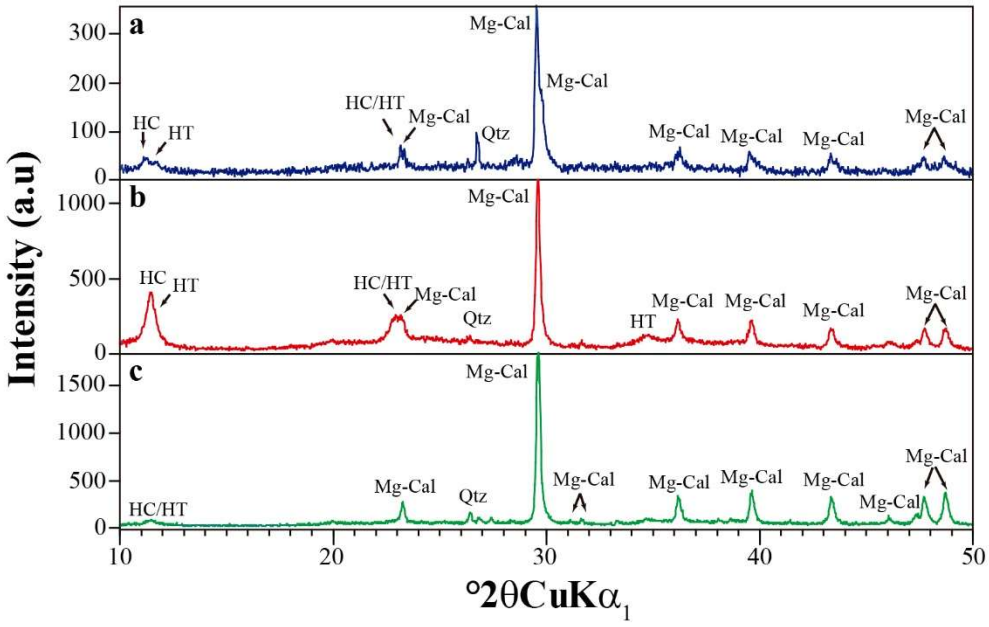

Figure 5. X-ray diffraction patterns of extracted binder fractions. (**a**) Fine fraction, (**b**) ultrafine fraction, and (**c**) target fraction. HC: hydrocalumite, HT: hydrotalcite, Qtz: quartz, Mg-Cal: magnesium calcite.

These LDH mineral phases are formed as a result of the slaking process and identification and characterization is crucial due to their very high ability to fix carbonate anions [68]. During the rehydration process, CO_3^{2-} from the partial washing of unburnt fragments of limestone is fixed in the crystalline structure of HT-like minerals. The captured CO_3^{2-} introduces dead carbon in the system and ages the radiometric dates. A new step was introduced in the extraction procedure in order to remove the potential contaminant HT-like mineral phases in the ultrafine fraction (<0.5 μm).

SEM observations of fine fraction (<2 μm) of the binder confirm the presence of very small HT-like particles embedded in a calcitic matrix (Figure 6). Irregular and hexagonal crystals of <0.5 μm grain size, corresponding to Ca-enriched or Mg-enriched anion clays, can be observed in Figure 6b. The Energy Dispersive X-ray (EDX) analyses indicate that well-formed or euhedral crystals correspond to Ca-enriched HT-like particles (point 1 in Figure 7) while the irregular or anhedral crystals correspond to Mg-enriched HT-like particles (point 2 in Figure 7). Therefore, Ca-enriched particles correspond to hydrocalumite and Mg-enriched particles to hydrotalcite. In fact, hydrotalcite is more likely to be present as a non-well-formed phase compared with hydrocalumite [44]. The EDX analysis also shows the presence of silica that has been attributed to the presence of microcrystalline quartz. The SEM images of ultrafine fraction (<0.5 μm) show a homogeneous matrix composed only of hydrotalcite and hydrocalumite phases of a <0.5 μm grain size. The SEM-EDX analysis supports that the extraction of HT-like minerals from the fine fraction was successful (Figure 6c).

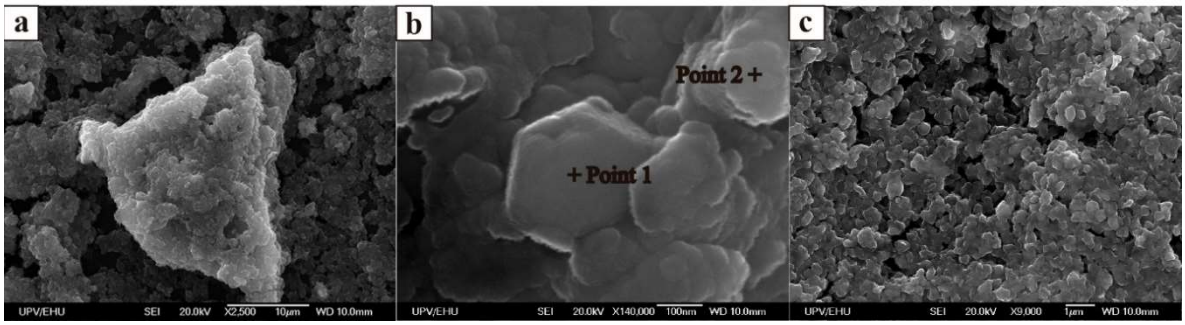

Figure 6. Scanning Electron Microscopy images of binder mortar: (**a**,**b**) fine fraction and (**c**) ultrafine fraction. Point 1 and point 2 indicate the particles analysed by EDX.

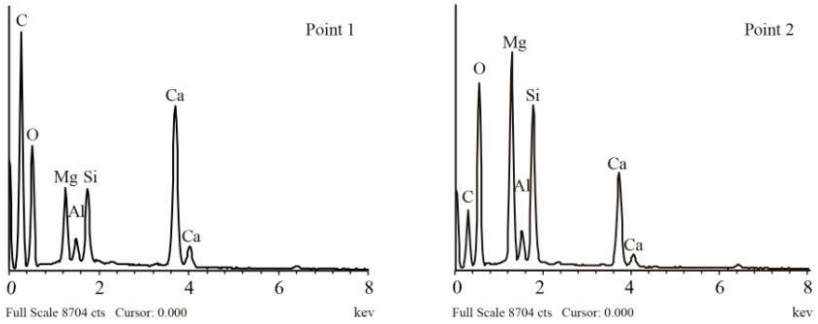

Figure 7. Energy dispersive X-ray analyses results of layered double hydroxides (LDH) of the fine fraction shown in Figure 6b. Point 1 is Ca-enriched anion clay (i.e., hydrocalumite) and point 2 is Ca-enriched anion clay (i.e., hydrotalcite).

Petrographic, XRD, and SEM-EDX analyses show that the raw material used to obtain lime was impure limestone and/or partially dolomitized limestone. When limestones enriched in calcium magnesium are calcined, magnesium minerals should be considered in the mortar binder. Magnesium oxide (MgO) is formed as well as calcium oxide (CaO) during the calcination of dolomitic rocks due to the dolomitic cycle, which differs from the typical lime cycle (Figure 8).

Considering that the LDH mineral phases constitute a potential contaminant in radiocarbon dating, the grain size fraction <0.5 μm (i.e., ultrafine fraction) is extracted in order to eliminate these phases. XRD patterns of UF show significant increases of reflexions at d = 7.86 Å (11.2° 2θ), d = 7.69 Å (11.4° 2θ), d = 3.83 Å (23.2° 2θ), and d = 2.58 Å (34.4° 2θ) corresponding to hydrotalcite and indicate a large enrichment of LDH mineral phases in the ultrafine fraction (Figure 5b).

As a result of the LDH minerals phase being removed, the target fraction (TF) corresponds to the grain size fraction between 0.5 μm to 2 μm. An XRD pattern of the TF fraction shows an increase in magnesium calcite reflections while hydrotalcite reflections disappear (Figure 5c). Nevertheless, an extraction procedure of the target fraction has to be checked in each mortar sample. Figure 9 shows XRD patterns of the target fraction of several samples. The presence and the intensity of characteristic reflections of LDH minerals in some XRD patterns suggest different levels of refinement in the extraction procedure, which indicates different amounts of LDH minerals in each sample. As can be observed, CP-2-TF, CP-4-TF, and CP-19-TF samples exhibit low intensity hydrotalcite reflections while CP-13-3-TF, CP-13-6-TF, CP-13-8-TF, and CP-13-10-TF samples still present significant LDH mineral reflections.

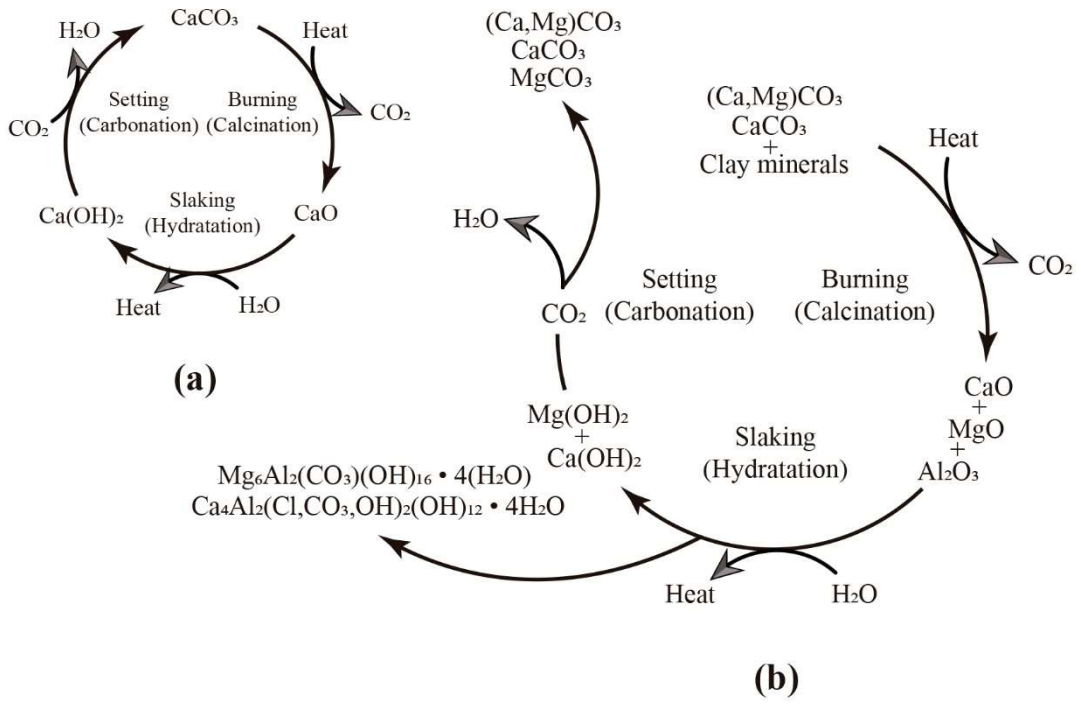

Figure 8. Lime binder cycles. (**a**) lime cycle and (**b**) proposal of dolomitic lime cycle of impure dolostone.

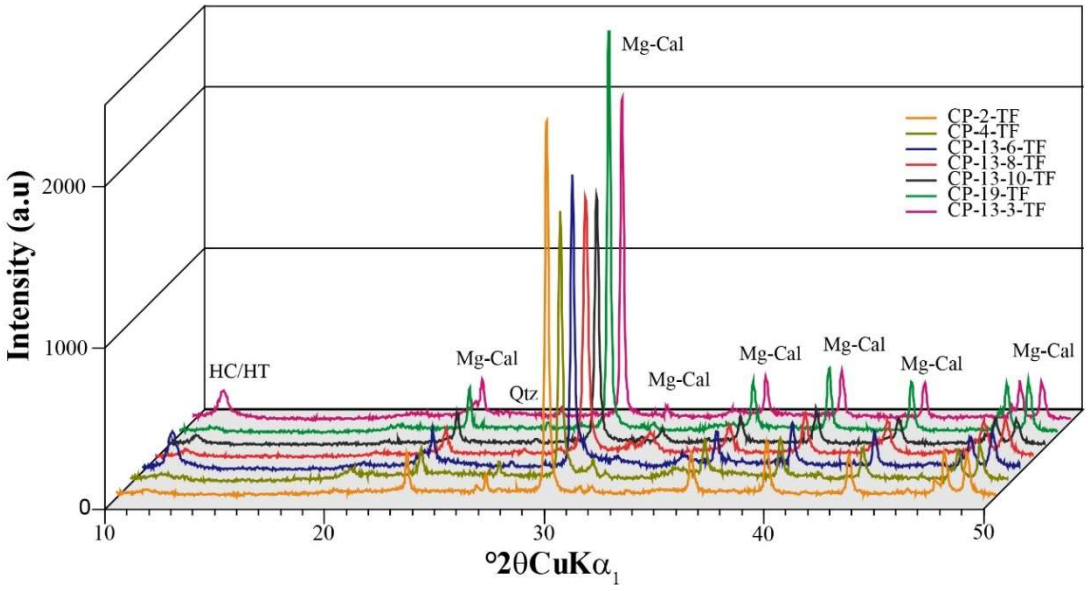

Figure 9. X-ray diffraction patterns of target fractions of different mortar binders. HC: hydrocalumite, HT: hydrotalcite, Mg-Cal: magnesium calcite, Qtz: quartz.

Table 2 summarizes the mineralogical assemblages and the semi-quantitative values (expressed in percentages) of identified phases in the ultrafine (<0.5 µm) and target (0.5 µm to 2 µm) factions. XRD results of target fraction show the persistent presence of LDH phases in small variable amounts in all samples. Nevertheless, XRD analysis does not always detect the presence of LDH phases when the amount remains near or under the detection limit. To check the extraction of the target fraction, even when the LDHs are not detected by XRD analysis, thermo-gravimetric analysis (TGA) is performed.

Table 2. Semi-quantitative data results (%) of X-ray diffraction analyses of target and ultrafine fractions of mortar binders.

Sample	Target Fraction (%)					Ultrafine Fraction (%)				
	Mg-Cal	HT	HC	Qtz	Total LDHs	Mg-Cal	HT	HC	Qtz	Total LDHs
CP-2	88	3	6	3	9	64	12	24	-	36
CP-4	84	8	8	-	16	58	16	26	-	42
CP-13-6	62	10	28	-	38	38	28	34	-	62
CP-13-8	79	9	10	2	19	48	28	24	-	52
CP-13-10	85	4	10	1	14	55	22	23	-	45
CP-19	89	5	5	1	10	55	24	20	-	44
CP-13-3	68	13	18	1	31	61	11	28	-	39

Mg-Cal: magnesium calcite, HT: hydrotalcite, HC: hydrocalumite, Qtz: quartz, LDHs: layered double hydroxides.

The temperature ranges and relative weight loss observed in TGA analysis are reliable for the characterization of these materials. The first weight loss below 120 °C is attributed to the presence of adsorption water in the inter-particle pore. The second weight loss occurs between 120 and 200 °C and is attributed to the crystallization water or the interlayer water. The weight loss between 200 °C to 600 °C is attributed to structural OH^-, which corresponds to the dehydration of the $Ca(OH)_2$ of pure carbonates. Lastly, at temperatures above 600 °C, the loss of CO_2 takes place due to the decomposition of the carbonate [69–71]. However, in the third decomposition step (200 °C to 600 °C) of target fraction (0.5 µm to 2 µm) from Portilla Castle samples, the TGA curve shows two weight loss steps (Figure 10). These weight losses correspond to the decomposition of LDH phases and are attributed to the loss of the OH^- groups bonded to Al^{3+} and to Mg^{2+} in Mg-Al-CO_3 compounds [72,73].

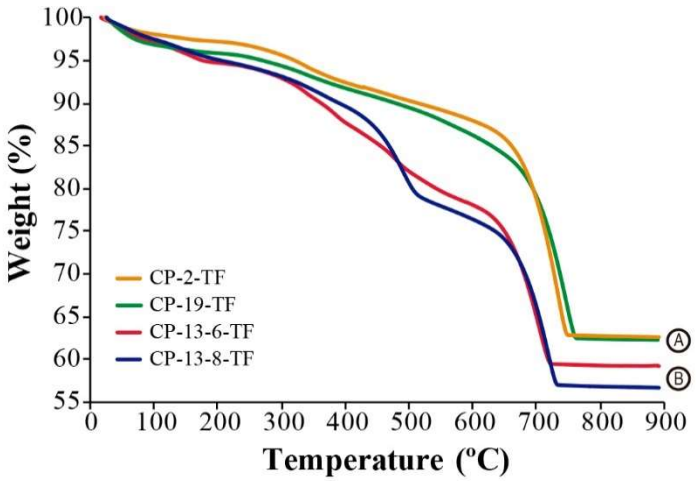

Figure 10. Thermo-gravimetric analyses of target fractions of representative mortar binders. (**A**) Binder samples with little weight loss and (**B**) binder samples with clear stepped weight loss in the 200 °C to 600 °C range.

The thermos-gravimetric analyses of the target fraction show two different patterns, which are representative of TGA curves. These patterns are shown in Figure 10. The pattern type-A corresponds to samples with little weight loss in the 200 °C to 600 °C range (CP-2-TF, CP-4-TF, and CP-19-TF) while pattern type-B displays a pronounced stepped weight loss (CP-13-3-TF, CP-13-6-TF, CP-13-8-TF, and CP-13-10-TF). Table 3 summarizes the weight loss percentages of the target fraction in each temperature range. Samples show weight loss between 1.5% and 2.9% due to adsorbed water. The lower weight loss of water molecules from the interlayer space corresponds to type-A patterns and higher to type-B patterns. The weight loss between 200 °C and 600 °C temperature range corresponding to the

dehydroxylation processes shows larger variations in the TG curves. Type-A pattern curves show weight loss varying from 10.3% to 12.8% while the weight loss in the type-B patterns varies from 13.6% to 19.6%. Weight loss in dehydroxylation processes shows larger contents of LDH minerals in the type-B samples than in samples with a type-A pattern. When over 600 °C, carbonates decompose and CO_2 content ranges between 16.3% and 23.5%. The weight loss of pure calcium carbonate decomposition is 44% and lower percentages of weight loss indicate variable amounts of other compounds as LDH minerals. Therefore, mortars with no or little structurally-bound water (OH^-) and high carbon dioxide content are potentially adequate for radiocarbon dating since they reflect the absence of other carbonate phases apart from calcite. Therefore, CP-2 and CP-19 are the most suitable mortars for radiocarbon dating since they display lower structurally-bound water and higher carbon dioxide content (Table 3).

Table 3. Thermo-gravimetric analysis results (wt %) of target fractions of mortar binders.

Sample	Pattern Type	$H_2O_{(Itp)}$	$H_2O_{(Itl)}$	OH^-	CO_3^{2-}
CP-2-TF	A	1.46	1.35	10.40	23.47
CP-4-TF	A	2.86	1.82	12.8	16.28
CP-13-6-TF	B	2.30	2.78	19.64	18.46
CP-13-8-TF	B	1.89	2.28	15.41	23.04
CP-13-10-TF	B	1.89	2.12	17.01	21.83
CP-19-TF	A	2.54	1.41	10.31	23.29
CP-13-3-TF	B	2.77	2.45	13.56	18.06

Itp: interparticle, Itl: interlayer, TF: target fraction. Pattern type as referred in Figure 10.

Since sample CP-19 shows the lowest weight loss of structurally-bound water corresponding to the decomposition of LDH phases, it has been selected instead of sample CP-2. In order to verify the contaminant potential of LDHs, both fine fraction (particle size <2 μm) and target fraction (particle size between 0.5 and 2 μm) have been dated (Table 4).

Table 4. Results of AMS ^{14}C dates for different grain-size fractions of mortar binder.

Lab Code	Sample	Binder Grain-Size	Conventional Age	$\delta^{13}C$	Calibrate Age (95.4%)
BETA375404	CP-19-TF	0.5–2 μm	1370 ± 30 BP	−16.5	Cal AD 640–675
BETA343295	CP-19-FF	<2 μm	2180 ± 40 BP	−21.3	Cal BC 380–160

TF: target fraction, FF: fine fraction.

The result of ^{14}C dating of CP-19-FF is 2180 ± 40 BP corresponding to the calendar age of Cal BC 380–160 (Figure 11a) and the radiocarbon age of CP-19-TF is 1370 ± 30 BP, which corresponds to the calendar age of Cal AD 640–675 (Figure 11b). The obtained dates are older than expected since the first written chronicle of Portilla Castle is dated in 1040 AD. The age interval between the archaeological age and radiocarbon ages of the target fraction reflects the persistent presence of dead carbon contamination related with the CO_3^{2-} anion of hydrotalcite and hydrocalumite.

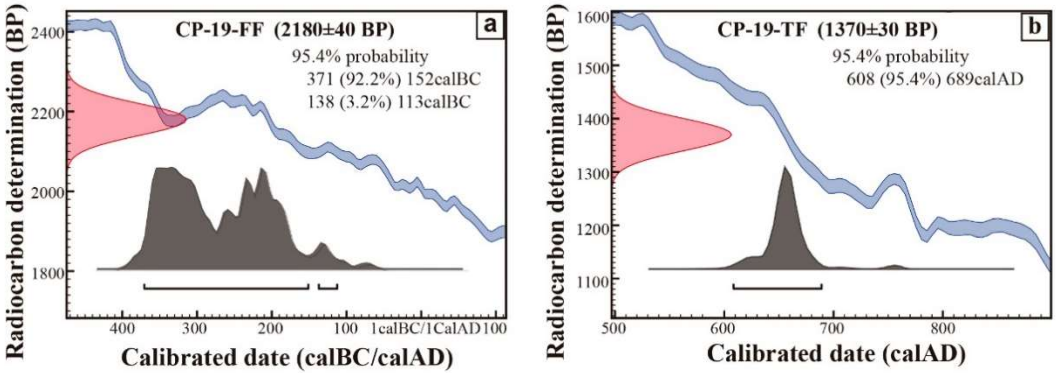

Figure 11. Calibrated ^{14}C dates of two fraction-sizes of the same lime mortar from Portilla Castle, (**a**) fine fraction (FF), and (**b**) target fraction (TF) obtained with OxCal v 4.1.7 [63] and IntCal09 atmospheric data [64].

The mineralogical composition of carbonate phases of the mortar binder and the granulometric distribution has determined the particle size to be extracted for radiocarbon dating. The selection of fine-grain size fraction (<2 μm) is only useful when the mortar binder is formed solely by calcite, e.g., Ortega et al. [28]. In contrast, when the binder includes hydrotalcite and hydrocalumite besides neo-formation calcite, as in Portilla Castle, which determines the granulometric distribution of carbonate minerals is essential in selecting effective thresholds. Once the granulometric distribution is determined, the most suitable preconditioning method should be established for each sample in order to isolate the adequate fraction for radiocarbon dating. Therefore, dating of mortars without a comprehensive mineralogical study can lead to meaningless results.

5. Conclusions

Portilla Castle mortars are formed by calcitic binder and quartz, limestone fragments, some partially dolomitized, and unburnt limestone remains as aggregates. The presence of hydrotalcite and hydrocalumite in the fine grain fraction of binder indicates the use of impure limestone and/or partially dolomitized limestones in the lime production. These raw materials provide magnesium and aluminium ions and under hyper-alkaline conditions lead to the formation of LDHs phases during the slaking process.

The continuous mineralogical control of the extraction procedure allows a better mineralogical characterization of the finest grain fractions (<2 μm) of the binder. Only the study of these fractions allows the identification of hydrotalcite and hydrocalumite in lime mortars. In this contribution, additional steps in the extraction process to remove small grain size particles enriched in LDHs has been performed making the obtained radiocarbon dates closer to the archaeological ages.

The occurrence of hydrotalcite and hydrocalumite mainly in the grain size is smaller than 0.5 μm in the Portilla Castle mortars, which adds dead carbon to the system and explains older ages than expected. Therefore, hydrotalcite and hydrocalumite constitute crucial contaminant mineral phases in mortar dating issues.

Mineralogical studies are essential to select the samples for dating and reject unsuitable samples since they allow the mineralogical nature of the contaminants and the grain size distribution within the binder to be determined. Mineralogical studies of the binder have to develop tailored purification procedures for each sample.

Author Contributions: L.A.O. and M.C.Z. conceived and designed the experiments; J.L.S., G.P-A. and L.A.O. selected archaeological materials, G.P.-A. performed the experiments; G.P.-A., L.A.O. and M.C.Z. analyzed the data; A.A.-O. contributed to the discussion; G.P.-A., L.A.O. and M.C.Z. wrote the paper.

Funding: This research was possible thanks to the financial support of SAI13/106 research project of Basque Country Government.

Acknowledgments: The authors would like to thank the anonymous referees for their comments and suggestions on the manuscript. GPA also acknowledges the PhD research grant of the Basque Country Government (2015-1-02-35). They also would like to thank Peter Smith for reviewing the use of English in the manuscript.

Conflicts of Interest: The authors declare no conflict of interest.

References

1. Schiffer, M. *Radiocarbon Dating and the "Old Wood" Problem: The Case of the Hohokam Chronology*; Elsevier: New York, NY, USA, 1986; Volume 13, pp. 13–30.
2. Mc Fadgen, B.G. Dating New Zealand archaeology by radiocarbon. *N. Z. J. Sci.* **1982**, *25*, 379–392.
3. Gavin, D.G. Estimation of inbuilt age in radiocarbon ages of soil charcoal for fire history studies. *Radiocarbon* **2001**, *43*, 27–44. [CrossRef]
4. Bowman, S. *Radiocarbon Dating*; British Museum Press: London, UK, 1990.
5. Taylor, R.; Bar-Yosef, O. *Radiocarbon Dating: An Archaeological Perspective*; Left Coast Press: Walnut Creek, CA, USA, 2014.
6. Boaretto, E.; Poduska, K.M. Materials science challenges in radiocarbon dating: The case of archaeological plasters. *J. Mater.* **2013**, *65*, 481–488. [CrossRef]
7. Kingery, D.W.; Pamela, B.V.; Martha, P. *The Beginnings of Pyrotechnology, Part II: Production and Use of Lime and Gypsum Plaster in the Pre-Pottery Neolithic Near East*; Taylor and Francis: New York, NY, USA, 1988; Volume 15, pp. 219–243.
8. Labeyrie, J.; Delibrias, G. Dating of old mortar by Carbon-14 method. *Nature* **1964**, *201*, 742–743. [CrossRef]
9. Stuiver, M.; Smith, C.S. *Radiocarbon Dating of Ancient Mortar and Plaster, Proceedings of the 6th International ^{14}C Conference, Montreal, Canada, 8–15 September 1965*; Chatters, R.M., Olson, C.A., Eds.; Clearinghouse for Federal Scientific and Technical Information: Springfield, IL, USA; pp. 338–343.
10. Pachiaudi, C.; Marechal, J.; Van Strydonck, M.; Dupas, M.; Dauchotdehon, M. Isotopic fractionation of carbon during CO_2 absorption by mortar. *Radiocarbon* **1986**, *28*, 691–697. [CrossRef]
11. Ambers, J. Stable carbon isotope ratios and their relevance to the determination of accurate radiocarbon dates for lime mortars. *J. Archaeol. Sci.* **1987**, *14*, 569–576. [CrossRef]
12. Baxter, M.S.; Walton, A. Radiocarbon dating of mortars. *Nature* **1970**, *225*, 937–938. [CrossRef] [PubMed]
13. Folk, R.L.; Valastro, S.J. Successful technique for dating of lime mortar by carbon-14. *J. Field Archaeol.* **1976**, *3*, 203–208. [CrossRef]
14. Van Strydonck, M.; Dupas, M.; Dauchot-Dehon, M. *Radiocarbon dating of old mortars, ^{14}C and Archaeology, Proceedings*; Mook, W.G., Waterbolk, H.T., Eds.; PACT: Phnom Penh, Cambodia, 1983; pp. 337–343.
15. Van Strydonck, M.; Dupas, M.; Dauchotdehon, M.; Pachiaudi, C.; Marechal, J. The influence of contaminating (fossil) carbonate and the variations of delta-C-13 in mortar dating. *Radiocarbon* **1986**, *28*, 702–710. [CrossRef]
16. Van Strydonck, M.J.Y.; Van der Borg, K.; De Jong, A.F.M.; Keppens, E. Radiocarbon dating of lime fractions and organic material from buildings. *Radiocarbon* **1992**, *34*, 873–879. [CrossRef]
17. Lindroos, A.; Heinemeier, J.; Ringbom, Å.; Braskén, M.; Sveinbjörnsdóttir, Á. Mortar dating using AMS ^{14}C and sequential dissolution: Examples from medieval, non-hydraulic lime mortars from the Åland Islands, SW Finland. *Radiocarbon* **2007**, *49*, 47–67. [CrossRef]
18. Sonninen, E.; Jungner, H. An improvement in preparation of mortar for radiocarbon dating. *Radiocarbon* **2001**, *43*, 271–273. [CrossRef]
19. Hale, J.; Heinemeier, J.; Lancaster, L.; Lindroos, A.; Ringbom, Å. Dating ancient mortar. *Am. Sci.* **2003**, *91*, 130–137. [CrossRef]
20. Nawrocka, D.; Michniewicz, J.; Pawlyta, J.; Pazdur, A. Application of radiocarbon method for dating of lime mortars. *Geochronometria* **2005**, *24*, 109–115.
21. Heinemeier, J.; Jungner, H.G.; Lindroos, A.; Ringbom, S.; von Konow, T.; Rud, N. AMS ^{14}C dating of lime mortar. *Nucl. Instrum. Methods Phys. Res. Sect. B Beam Interact. Mater. Atoms* **1997**, *123*, 487–495. [CrossRef]
22. Tubbs, L.E.; Kinder, T.N. The use of AMS for the dating of lime mortars. *Nucl. Instrum. Methods Phys. Res. Sect. B Beam Interact. Mater. Atoms.* **1990**, *52*, 438. [CrossRef]
23. Toffolo, M.; Maeir, A.M.; Chadwick, J.R.; Boaretto, E. Characterization of contexts for radiocarbon dating: Results from the early Iron Age at Tell es-Safi/Gath, Israel. *Radiocarbon* **2012**, *54*, 371–390. [CrossRef]

24. Asscher, Y.; Lehmann, G.; Rosen, S.A.; Weiner, S.; Boaretto, E. Absolute dating of the late bronze to iron age transition and the appearance of philistine culture in qubur el-walaydah, southern Levant. *Radiocarbon* **2015**, *57*, 77–97. [CrossRef]
25. Rodriguez-Navarro, C.; Hansen, E.; Ginell, W.S. Calcium hydroxide crystal evolution upon aging of lime putty. *J. Am. Ceram. Soc.* **1998**, *81*, 3032–3034. [CrossRef]
26. Boynton, R.S. *Chemistry and Technology of Lime and Limestone*; John Wiley & Sons, Inc.: New York, NY, USA, 1980.
27. Zouridakis, N.M.; Saliege, J.F.; Person, A.; Filippakis, S.E. Radiocarbon dating of mortars from ancient greek palaces. *Archaeometry* **1987**, *29*, 60–68. [CrossRef]
28. Ortega, L.A.; Zuluaga, M.C.; Alonso-Olazabal, A.; Murelaga, X.; Insausti, M.; Ibañez-Etxeberria, A. Historic lime-mortar ^{14}C dating of Santa María la Real (Zarautz, northern Spain): Extraction of suitable grain size for reliable ^{14}C dating. *Radiocarbon* **2012**, *54*, 23–36. [CrossRef]
29. Marzaioli, F.; Lubritto, C.; Nonni, S.; Passariello, I.; Capano, M.; Terrasi, F. Mortar radiocarbon dating: Preliminary accuracy evaluation of a novel methodology. *Anal. Chem.* **2011**, *83*, 2038–2045. [CrossRef] [PubMed]
30. Marzaioli, F.; Nonni, S.; Passariello, I.; Capano, M.; Ricci, P.; Lubritto, C.; De Cesare, N.; Eramo, G.; Quirós Castillo, J.A.; Terrasi, F. Accelerator mass spectrometry ^{14}C dating of lime mortars: Methodological aspects and field study applications at CIRCE (Italy). *Nucl. Instrum. Methods Phys. Res. Sect. B Beam Interact. Mater. Atoms* **2013**, *294*, 246–251. [CrossRef]
31. Folk, R.L.; Valastro, S. Successful Technique for Dating of Lime Mortar by Carbon-14. *J. Field Archaeol.* **1976**, *3*, 203–208. [CrossRef]
32. Goslar, T.; Nawrocka, D.; Czernik, J. Foraminiferous limestone in C-14 dating of mortar. *Radiocarbon* **2009**, *51*, 987–993. [CrossRef]
33. Heinemeier, J.; Ringbom, A.; Lindroos, A.; Sveinbjornsdottir, A.E. Successful AMS ^{14}C dating of non-hydraulic lime mortars from the medieval churches of the Aland Islands, Finland. *Radiocarbon* **2010**, *52*, 171–204. [CrossRef]
34. Al-Bashaireh, K. Plaster and mortar radiocarbon dating of Nabatean and Islamic structures, South Jordan. *Archaeometry* **2013**, *55*, 329–354. [CrossRef]
35. Ringbom, A.; Lindroos, A.; Heinemeier, J.; Sonck-Koota, P. 19 years of mortar dating: Learning from experience. *Radiocarbon* **2014**, *56*, 619–635. [CrossRef]
36. Nonni, S.; Marzaioli, F.; Secco, M.; Passariello, I.; Capano, M.; Lubritto, C.; Mignardi, S.; Tonghini, C.; Terrasi, F. ^{14}C mortar dating: The case of the medieval shayzar citadel, Syria. *Radiocarbon* **2013**, *55*, 514–525. [CrossRef]
37. Pesce, G.; Quarta, G.; Calcagnile, L.; D'Elia, M.; Cavaciocchi, P.; Lastrico, C.; Guastella, R. Radiocarbon dating of lumps from aerial lime mortars and plasters: Methodological issues and results from San Nicolò of Capodimonte church (Camogli, Genoa, Italy). *Radiocarbon* **2009**, *51*, 867–872. [CrossRef]
38. Pesce, G.L.A.; Ball, R.J.; Quarta, G.; Calcagnile, L. Identification, extraction, and preparation of reliable lime samples for ^{14}C dating of plasters and mortars with the "pure lime lumps" technique. *Radiocarbon* **2012**, *54*, 933–942. [CrossRef]
39. Beruto, D.T.; Vecchiattini, R.; Giordani, M. Solid products and rate-limiting step in the thermal half decomposition of natural dolomite in a CO_2 (g) atmosphere. *Thermochim. Acta* **2003**, *405*, 183–194. [CrossRef]
40. Schork, J. Dolomitic Lime in the US. *J. Archit. Conserv.* **2012**, *18*, 7–25. [CrossRef]
41. Kuzel, H.-J.; Baier, H. Hydration of calcium aluminate cements in the presence of calcium carbonate. *Eur. J. Mineral.* **1996**, 129–142. [CrossRef]
42. Evans, D.G.; Slade, R.C.T. Structural aspects of layered double hydroxides. In *Layered Double Hydroxides*; Duan, X., Evans, D.G., Eds.; Springer: Berlin/Heidelberg, Germany, 2006; pp. 1–87.
43. Forano, C.; Hibino, T.; Leroux, F.; Taviot-Guého, C. Chapter 13.1 layered double hydroxides. *Dev. Clay Sci.* **2006**, *1*, 1021–1095.
44. Guo, Q.; Reardon, E.J. Calcined dolomite: Alternative to lime for minimizing undesirable element leachability from fly ash. *Ind. Eng. Chem. Res.* **2012**, *51*, 9106–9116. [CrossRef]
45. Miyata, S.; Okada, A. Synthesis of hydrotalcite-like compounds and their physico-chemical properties—The systems Mg^{2+}-Al^{3+}-$SO_4{}^{2-}$- and Mg^{2+}-Al^{3+}-$CrO_4{}^{2-}$. *Clays Clay Min.* **1977**, *25*, 14–18. [CrossRef]

46. Miyata, S. Physico-chemical properties of synthetic hydrotalcites in relation to composition. *Clays Clay Min.* **1980**, *28*, 50–56. [CrossRef]
47. Miyata, S. Anion-exchange properties of hydrotalcite-like compounds. *Clays Clay Min.* **1983**, *31*, 305–311. [CrossRef]
48. Reichle, W.T. Synthesis of anionic clay minerals (mixed metal hydroxides, hydrotalcite). *Solid State Ionics* **1986**, *22*, 135–141. [CrossRef]
49. Cavani, F.; Trifirò, F.; Vaccari, A. Hydrotalcite type anionic clays, preparation, properties and applications. *Catal. Today* **1991**, *11*, 173–301. [CrossRef]
50. Mills, S.J.; Christy, A.G.; Génin, J.-M.R.; Kameda, T.; Colombo, F. Nomenclature of the hydrotalcite supergroup: Natural layered double hydroxides. *Mineral. Mag.* **2012**, *76*, 1289–1336. [CrossRef]
51. Kutus, B.; Gacsi, A.; Pallagi, A.; Palinko, I.; Peintler, G.; Sipos, P. A comprehensive study on the dominant formation of the dissolved $Ca(OH)_2$ (aq) in strongly alkaline solutions saturated by Ca(ii). *RSC Adv.* **2016**, *6*, 45231–45240. [CrossRef]
52. Pallagi, A.; Tasi, A.; Gácsi, A.; Csáti, M.; Pálinkó, I.; Peintler, G.; Sipos, P. The solubility of $Ca(OH)_2$ in extremely concentrated NaOH solutions at 25 °C. *Cent. Eur. J. Chem.* **2012**, *10*, 332–337. [CrossRef]
53. Reardon, E.J.; Della Valle, S. Anion sequestering by the formation of anionic clays: Lime treatment of fly ash slurries. *Environ. Sci. Technol.* **1997**, *31*, 1218–1223. [CrossRef]
54. Rosenberg, S.P.; Armstrong, L. Layered double hydroxides in the Bayer process: Past, present and future. In *Essential Readings in Light Metals*; Springer: Berlin, Germany, 2005; pp. 157–161.
55. Sipos, P. The structure of Al (III) in strongly alkaline aluminate solutions—A review. *J. Mol. Liq.* **2009**, *146*, 1–14. [CrossRef]
56. Gácsi, A.; Kutus, B.; Kónya, Z.; Kukovecz, Á.; Pálinkó, I.; Sipos, P. Estimation of the solubility product of hydrocalumite-hydroxide, a layered double hydroxide with the formula of $[Ca_2Al(OH)_6]OH{\cdot}nH_2O$. *J. Phys. Chem. Solids* **2016**, *98*, 167–173. [CrossRef]
57. Artioli, G.; Secco, M.; Addis, A.; Bellotto, M. 5 Role of hydrotalcite-type layered double hydroxides in delayed pozzolanic reactions and their bearing on mortar dating. In *Cementitious Materials: Composition, Properties, Application*; Walter de Gruyter: Berlin, Germany, 2017.
58. Siedel, H.; Michalski, S.; Ullrich, B. Characterisation of dolomitic lime mortars from the Benedictine monastery in Riesa, Saxony (Germany). In *Historic Mortars*; Springer: Dordrecht, The Netherlands, 2012; pp. 115–124.
59. Brandon, C.J.; Hohlfelder, R.L.; Jackson, M.D.; Oleson, J.P. *Building for Eternity: The History and Technology of Roman Concrete Engineering in the Sea*; Oxbow Books: Oxford, UK; Philadelphia, PA, USA, 2014.
60. Massazza, F. Pozzolana and pozzolanic cements. In *Lea's Chemistry of Cement and Concrete*, 4th ed.; Hewlett, P., Ed.; Elsevier-Butterworth-Heinemann: Oxford, UK, 1998; pp. 471–635.
61. Sagredo, I. *Navarra: Castillos que Defendieron el Reino (Tomo III) La Navarra Occidental, la Frontera del Mar Álava, Bizkaia, el Duranguesado, Guipuzkoa*; PAMIELA: Pamplona, Spain, 2007.
62. Solaun, J.L.; Azcárate, A. El castillo de Portilla (Zambrana, Alava). Origen y significado de una fortaleza plenomedieval en territorio alavés (siglos XI-XII). *Munibe Antropol.-Arkeol.* **2016**, *67*, 167–183.
63. Ramsey, C.B.; Scott, M.; van der Plicht, H. Calibration for archaeological and environmental terrestrial samples in the time range 26–50 ka cal BP. *Radiocarbon* **2013**, *55*, 2021–2027. [CrossRef]
64. Reimer, P.J.; Bard, E.; Bayliss, A.; Beck, J.W.; Blackwell, P.G.; Ramsey, C.B.; Buck, C.E.; Cheng, H.; Edwards, R.L.; Friedrich, M.; et al. IntCal13 and marine13 radiocarbon age calibration curves 0–50,000 years cal BP. *Radiocarbon* **2013**, *55*, 1869–1887. [CrossRef]
65. Casadio, F.; Chiari, G.; Simon, S. Evaluation of binder/aggregate ratios in archaeological lime mortars with carbonate aggregate: A comparative assessment of chemical, mechanical and microscopic approaches. *Archaeometry* **2005**, *47*, 671–689. [CrossRef]
66. Warkentin, B.P.; Maeda, T. Physical and mechanical characteristics of andisols. In *Soils with Variable Charge*; Theng, B.K.G., Ed.; New Zealand Society of Soil Science: Lower Hutt, New Zealand, 1980; pp. 281–302.
67. Langmuir, D. *Aqueous Environmental Geochemistry*; Prentice Hall: London, UK, 1997.
68. Grover, K.; Komarneni, S.; Katsuki, H. Synthetic hydrotalcite-type and hydrocalumite-type layered double hydroxides for arsenate uptake. *Appl. Clay Sci.* **2010**, *48*, 631–637. [CrossRef]
69. Bakolas, A.; Biscontin, G.; Moropoulou, A.; Zendri, E. Characterization of structural byzantine mortars by thermogravimetric analysis. *Thermochim. Acta* **1998**, *321*, 151–160. [CrossRef]

70. Paama, L.; Pitkänen, I.; Rönkkömäki, H.; Perämäki, P. Thermal and infrared spectroscopic characterization of historical mortars. *Thermochim. Acta* **1998**, *320*, 127–133. [CrossRef]
71. Moropoulou, A.; Bakolas, A.; Anagnostopoulou, S. Composite materials in ancient structures. *Cem. Concr. Compos.* **2005**, *27*, 295–300. [CrossRef]
72. Yang, W.; Kim, Y.; Liu, P.K.T.; Sahimi, M.; Tsotsis, T.T. A study by in situ techniques of the thermal evolution of the structure of a Mg-Al-CO_3 layered double hydroxide. *Chem. Eng. Sci.* **2002**, *57*, 2945–2953. [CrossRef]
73. León, M.; Díaz, E.; Bennici, S.; Vega, A.; Ordóñez, S.; Auroux, A. Adsorption of CO_2 on hydrotalcite-derived mixed oxides: Sorption mechanisms and consequences for adsorption irreversibility. *Ind. Eng. Chem. Res.* **2010**, *49*, 3663–3671. [CrossRef]